



This is the accepted manuscript made available via CHORUS, the article has been published as:

# Complex quantum network model of energy transfer in photosynthetic complexes

Bao-quan Ai and Shi-Liang Zhu

Phys. Rev. E **86**, 061917 — Published 28 December 2012

DOI: [10.1103/PhysRevE.86.061917](https://doi.org/10.1103/PhysRevE.86.061917)

# Complex quantum network model of excitation energy transfer in photosynthetic complexes

Bao-quan Ai<sup>1</sup> and Shi-Liang Zhu<sup>1,\*</sup>

<sup>1</sup>*Laboratory of Quantum Information Technology and SPTE,  
South China Normal University, Guangzhou, China*

## Abstract

The quantum network model with real variables is usually used to describe the excitation energy transfer (EET) in the Fenna-Matthews-Olson(FMO) complexes. In this paper we add the quantum phase factors to the hopping terms and find that the quantum phase factors play an important role in the EET. The quantum phase factors allow us to consider the space structure of the pigments. It is found that phase coherence within the complexes would allow quantum interference to affect the dynamics of the EET. There exist some optimal phase regions where the transfer efficiency takes its maxima, which indicates that when the pigments are optimally spaced, the exciton can pass through the FMO with perfect efficiency. Moreover, the optimal phase regions almost do not change with the environments. In addition, we find that the phase factors are useful in the EET just in the case of multiple-pathway. Therefore, we demonstrate that, the quantum phases may bring the other two factors, the optimal space of the pigments and multiple-pathway, together to contribute the EET in photosynthetic complexes with perfect efficiency.

PACS numbers: 87.15.A-; 71.35.-y; 87. 15. hj

---

\*Electronic address: [shilzhu@yahoo.com.cn](mailto:shilzhu@yahoo.com.cn)

## I. INTRODUCTION

Photosynthesis provides chemical energy for almost all life on Earth. The initial step of photosynthesis involves absorption of light by the so-called light-harvesting antennae complexes, and funneling of the resulting electronic excitation to the photosynthetic reaction center. Recent work has reported that quantum theory governs the exciton transfer in some light-harvesting complexes that harness the absorbed energy with almost 100% efficiency [1–7]. The experimental evidence [2–6] showing long-lived quantum coherences in this energy transport in several photosynthetic light harvesting complexes suggests that coherence may play an important role in the function of these systems. These observations have generated considerable interest in understanding the possibly functional role of quantum coherence effects in the remarkably efficient excitation energy transfer in photosynthetic complexes.

The experimental achievements have motivated a number of theoretical works [8–30] that consider the photosynthetic complex as a quantum system, and try to analyze the basic mechanisms that explain the phenomena observed in the experiments. A full quantum dynamic framework becomes necessary for studying coherent energy transfer. Typical quantum theories are, the quantum network model [8–20], the hierarchic equation [21–24], the generalized Bloch-Redfield [25] equation, **the renormalization group methods** [26], and the mixed quantum-classical method[30]. **Some recent theories [31] can even successfully predict the long-lived quantum coherent phenomenon.** However, all these models cannot describe the space distribution of the pigments. As we know, the space distribution of the pigments is very important for exciton energy transfer and the experimental evidence also shows that the optimized space distribution of the pigments is one factor for perfect energy transfer in light-harvesting complexes [2, 3]. Therefore, it is necessary to set up a quantum model in which the space distribution of the pigments is considered.

In this paper, we set up a quantum network model by adding the quantum phase factors to the two-body interactions to describe the exciton (the energy carrier) transfer in the FMO complex. The quantum phases are determined by the spatial structure of the pigments in photosynthetic complexes, such as the length of the pigment, the barriers and the distance between pigments. The quantum network in the absence of the phase factors has been used

to study the EET in the photosynthetic complexes[8–18]. Some interesting results, such as the noises may enhance the EET, the EET in a quantum model may be larger than that of a classical model, are obtained. Compared with those studies, we find that the newly added quantum phase factors play a key role in the EET and there exist optimized phases at which the transfer efficiency is maximal. Furthermore, we find that the phase factors affect the EET just in the form of the phase difference in a closed loop. Although there may be many phase factors in the coupling terms of the system Hamiltonian, only  $N_p - 1$  are independent variables where  $N_p$  is the number of the pathways. **This conclusion stems from the fundamental property of a quantum phase: only a gauge invariant phase is observable, while quantum phase accumulated in a closed path is such an invariant. As for  $N_p$  pathways, there exist  $N_p - 1$  closed paths.** So it implies that multiple-pathway in FMO complexes is a necessary condition for the enhancement of the EET by the quantum phases. It provides a strong evidence to support the statement that the multiple energy delivery pathway is also an acceptable contributing factor for perfect energy transfer[2, 3]. Therefore, we demonstrate that, the quantum phases may bring the other two factors, the optimal space of the pigments and multiple-pathway, together to contribute the EET in photosynthetic complexes with perfect efficiency.

The paper is organized as follows. In sec. II, we present the complex quantum network we used to study the EET in photosynthetic complexes. A particularly simple and illustrative example with three sites of complex network is presented in sec. III, where some main conclusions, such as the phases may play an important role in the EET and the optimized phases are insensitive to the environments, are demonstrated in this very simple example. In sec. IV, we present a symmetric complex quantum network with  $N_p$  pathways to show that the multi-pathway is also a contributing factor for the perfect efficiency of the EET. In sec. V, we investigate the EET in FMO with our complex quantum network model. Finally, the conclusions are presented in sec. VI.

## II. THE QUANTUM NETWORK MODEL WITH THE PHASES

The system we consider is a quantum network of  $N$  connected sites (nodes), schematically shown in Fig.1. Each site is modelled here as a spin-1/2 particle and it may support an excitation which can be exchanged between lattice sites by hopping. The initial (input) state

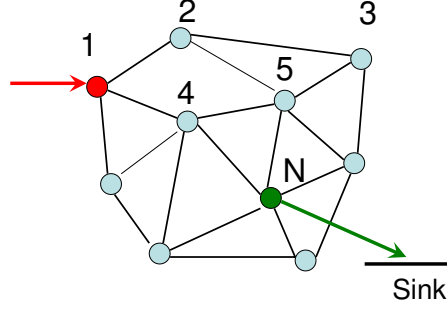


FIG. 1: (Color online) The schematic representation of the quantum network which are a collection of  $N$  connected sites (nodes). Each site is modelled as a spin-1/2 particle (qubit). The particles are interacting with each other (solid lines) in the quantum network and may suffer dissipative losses as well as dephasing. An excitation is initialled at site 1. The arrow between site  $N$  and sink denotes an irreversible transfer of excitations from site  $N$  to the sink.

is an excitation state which describes an excitation localized at site 1 (or several sites). We are interested to the transfer rate that the excitation transfers from the input state to the sink. The quantum evolution of the network of  $N$  sites is usually described by a Hamiltonian of the form

$$H = \sum_{j=1}^N \epsilon_j \sigma_j^+ \sigma_j^- + \sum_{j \neq l} V_{jl} (\sigma_j^+ \sigma_l^- + \sigma_l^+ \sigma_j^-), \quad (1)$$

where  $\sigma_j^+$  and  $\sigma_j^-$  are the raising and lowering operators for site  $j$ .  $\sigma_j^+ = |j\rangle\langle 0|$  and  $\sigma_j^- = |0\rangle\langle j|$ , where  $|0\rangle$  represents the zero exciton state of the system and  $|j\rangle$  denotes the excitation being at the site  $j$ . The site energy and two-body coupling strength are given by the real numbers  $\epsilon_j$  and  $V_{jl}$ , respectively. The quantum network[32] described in Eq.(1) has been used to study the EET in photosynthetic complexes in many literature [8–17].

In this paper, we add a quantum phase factor  $e^{-i\phi_{jl}}$  with  $\phi_{jl}$  a real number to the hopping term between sites  $j$  and  $l$ . The phase factor is determined by the detailed structure of the quantum network. As for the FMO, the phases are related to the length of the pigments as well as the intrinsic features of the barriers between the adjacent pigments. In this case, the Hamiltonian (1) is replaced by

$$H = \sum_{j=1}^N \epsilon_j \sigma_j^+ \sigma_j^- + \sum_{j \neq l} V_{jl} (e^{-i\phi_{jl}} \sigma_j^+ \sigma_l^- + e^{i\phi_{jl}} \sigma_l^+ \sigma_j^-). \quad (2)$$

Compared with the quantum network with real variables in Eq(1). This model can be named as a complex quantum network model. We will show that the quantum phase factors paly

the fundamental role in energy transfer of the photosynthetic complexes.

As usual, we assume that all sites are susceptible simultaneously to two distinct types of noise processes. The first one is a dissipative process that transfers the excitation energy in site  $j$  to the environment with rate  $\Gamma_j$ , which leads to energy loss. The second one is a pure dephasing process with rate  $\gamma_j$  which destroys the phase coherence of any superposition state in the system. The dissipative and the pure dephasing processes are described, respectively, by the Lindblad super-operators [9–11],

$$L_{diss}(\rho) = \sum_{j=1}^N \Gamma_j [-\{\sigma_j^+ \sigma_j^-, \rho\} + 2\sigma_j^- \rho \sigma_j^+], \quad (3)$$

$$L_{deph}(\rho) = \sum_{j=1}^N \gamma_j [-\{\sigma_j^+ \sigma_j^-, \rho\} + 2\sigma_j^+ \sigma_j^- \rho \sigma_j^+ \sigma_j^-], \quad (4)$$

where  $\{A, B\}$  is an anticommutator. The absorption of the energy from the site  $k$  to the sink (numbered  $s$ ) is modeled by a Lindblad operator

$$L_s(\rho) = \Gamma_s [2\sigma_s^+ \sigma_k^- \rho \sigma_k^+ \sigma_s^- - \{\sigma_k^+ \sigma_s^- \sigma_s^+ \sigma_k^-, \rho\}], \quad (5)$$

where  $\Gamma_s$  is the trapping rate. This term describes the irreversible decay of the excitations to the sink. So the full time evolution of the density matrix  $\rho$  of the system is described by the master equation

$$\frac{d\rho}{dt} = -\frac{i}{\hbar} [H, \rho] + L_{diss}(\rho) + L_{deph}(\rho) + L_s(\rho). \quad (6)$$

The efficiency of EET is measured by the population  $P_{sink}$  transferred to the sink from the site  $k$  [9–11],

$$P_{sink} = \rho_{sink}(\infty) = 2\Gamma_s \int_0^\infty \rho_{kk}(t) dt. \quad (7)$$

### III. BI-PATHWAY QUANTUM NETWORK

To study the role of the phase in quantum network, a particularly simple and illustrative example shown in Fig. 2 is to study quantum transport in a system of three sites.

The exciton is transferred from site 1 to site 3 through two pathways, and finally, is trapped by the sink with the rate  $\Gamma_s$ . The sites 1, 2, and 3 are susceptible simultaneously to the dissipative and the pure dephasing processes. The dynamics of the system can

be described by Eqs. (2-7). If we choose  $\epsilon_1 = \epsilon_2 = \epsilon_3 = \epsilon$ ,  $V_{12} = V_{23} = V_{13} = V$ ,  $\Gamma_1 = \Gamma_2 = \Gamma_3 = \Gamma$ ,  $\gamma_1 = \gamma_2 = \gamma_3 = \gamma$ , the analytical expression of  $P_{sink}$  (in the Appendix) can be obtained

$$P_{sink} = \frac{V^4 \Gamma_s [A^2 V^4 \sin^2 \phi - AV \Gamma (DB^2 + AV^2) \sin \phi + BD(D\Gamma B^2 + ACV^2)]}{A^2 V^6 (3\Gamma + \Gamma_s) \sin^2 \phi + G}, \quad (8)$$

where the phase difference  $\phi = \phi_{12} + \phi_{23} - \phi_{13}$ ,  $G = (D\Gamma B^2 + ACV^2)[D\Gamma(\Gamma + \Gamma_s)B^2 + C(2\Gamma\Gamma_s + \gamma\Gamma_s + 3D\Gamma)V^2]$ ,  $A = 3\Gamma + \Gamma_s + 3\gamma$ ,  $B = 2\Gamma + \Gamma_s + 2\gamma$ ,  $C = 3\Gamma + \Gamma_s + 2\gamma$ , and  $D = \Gamma + \Gamma_s$ . **Note that the corresponding analytical expression of  $P_{sink}$  for the real coupling rates is obtained in Ref. [8].** Although there are three phase factors  $\phi_{12}$ ,  $\phi_{23}$ , and  $\phi_{13}$  in this three-site network, it is notable that only the phase difference  $\phi = \phi_{12} + \phi_{23} - \phi_{13}$  is independent. It demonstrates the fact that only the phase difference accumulated in the two pathways ( the pathway  $1 \rightarrow 2 \rightarrow 3$  and pathway  $1 \rightarrow 3$  ) affects the interference at site 3.

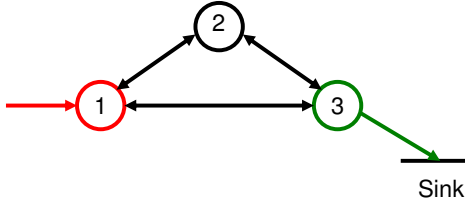


FIG. 2: (Color online) The schematic representation of a bi-pathway quantum network. The exciton is transferred from site 1 to site 3 through two pathways, and finally, is trapped by the sink with the rate  $\Gamma_s$ .

From Eq. (8), we can easily find that  $P_{sink}$  always increases with  $V$ , while it always decreases with  $\Gamma$ . However,  $P_{sink}$  is not monotonic functions of  $\gamma$  and  $\Gamma_s$ . We plot the dependence of  $P_{sink}$  on the different parameters in Fig.3.

Figure 3(a) shows the relation between  $P_{sink}$  and  $\gamma$  for different values of  $\phi$ . For  $\phi = 0$ , there exists an optimal value of  $\gamma$  at which  $P_{sink}$  is maximal, which indicates that the dephasing from the noise may even facilitate the EET. Note that the similar conclusion is extensively reported in the previous works [9, 10, 16]. When the phase  $\phi$  is considered, the phase can change the efficiency remarkably at low dephasing (purely quantum mechanical), while the efficiency is not sensitive to the phase at large dephasing (quantum coherent destroyed). Therefore, the phase in EET plays a key role at low dephasing.

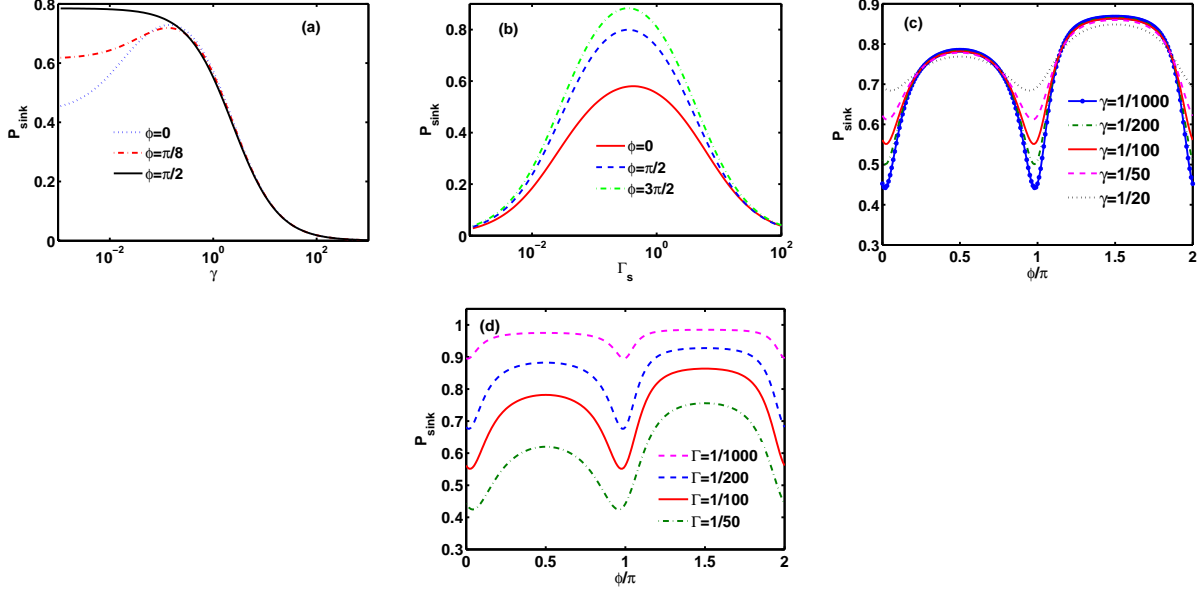


FIG. 3: (Color online) The dependence of the transfer efficiency  $P_{sink}$  on the different parameters. (a)  $P_{sink}$  vs  $\gamma$  for different values of  $\phi$ . (b)  $P_{sink}$  vs  $\Gamma_s$  for different values of  $\phi$ . (c)  $P_{sink}$  vs  $\phi$  for different values of  $\gamma$ . (d)  $P_{sink}$  vs  $\phi$  for different values of  $\Gamma$ . Unless otherwise noted, the parameters are  $V = 1/5$ ,  $\Gamma_s = 1/5$ ,  $\Gamma = 1/100$ , and  $\gamma = 1/100$ .

Figure 3(b) shows the dependence of the transfer efficiency  $P_{sink}$  on the trapping rate  $\Gamma_s$  for different values of  $\phi$ . When  $\Gamma_s$  is very small, the system couples weakly to the sink, few exciton can reach the sink and the efficiency tends to zero. When  $\Gamma_s$  is too large, the trapping rate  $\Gamma_s$  mismatches the transport rate of the exciton in the quantum network, thus the efficiency also goes to zero. Therefore, there exists an optimal value of  $\Gamma_s$  at which the efficiency takes its maximal value.

Figure 3(c) and (d) show the efficiency  $P_{sink}$  as a function of the phase  $\phi$  for different values of  $\gamma$  and  $\Gamma$ , respectively. It is found that there are two optimal values (about  $\pi/2$  and  $3\pi/2$ ) of  $\phi$  at which  $P_{sink}$  takes its extremum value, especially, it reaches a maximum value at  $3\pi/2$ . The minimal value of  $P_{sink}$  appears at  $\phi \approx 0, \pi$  and  $2\pi$ . Obviously, the maximal values of  $P_{sink}$  are due to the constructive interference, while its minimal values are due to the destructive interference. Interestingly, the phases which correspond to the extremal values of  $P_{sink}$  almost do not change with  $\gamma$  and  $\Gamma$ .

Therefore, we can conclude that quantum phase in the two-body couplings plays a key

role in the EET, especially at low dephasing. Remarkably, the optimized phases in quantum network are almost independent of the environments ( $\gamma$  and  $\Gamma$ ).

#### IV. MULTIPLE-PATHWAY QUANTUM NETWORK

Since the number of the pathways is an important quantity in quantum network, it is necessary to investigate the role of the multiple pathways on the efficiency of EET. For simplicity, we consider a symmetric complex quantum network including  $N_p$  pathways shown in Fig. 4. The exciton is transferred from site  $I$  to site  $F$  through multiple pathways, and

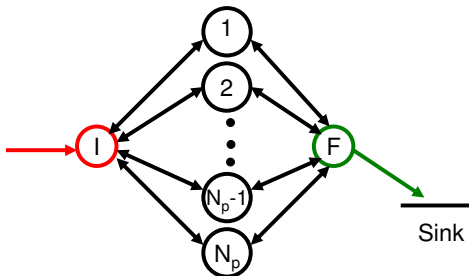


FIG. 4: (Color online) The schematic representation of the symmetric quantum network including  $N_p$  pathways. An excitation is initialised at site  $I$  and be transferred to site  $F$  through  $N$  pathways. The arrow between site  $F$  and sink denotes an irreversible transfer of excitations from site  $F$  to the sink.

finally, is trapped by the sink.  $N_p$  describes the number of the pathways between the sites  $I$  and  $F$ . The dynamics of the system can also be described by Eqs. (2-7). From Eqs. (2-7), we can obtain the efficiency  $P_{sink}$  for different number  $N_p$  of the pathways.

Figure 5 shows the dependence of the transfer efficiency  $P_{sink}$  on the phase  $\phi$  for different number  $N_p$  of the pathways. For a symmetric network, we choose  $\epsilon_j = \epsilon$ ,  $V_{Ij} = V_{Fj} = V$ ,  $\Gamma_j = \Gamma, \gamma_j = \gamma$ ,  $j = 1, 2, 3 \dots N_p$ . There are  $N_p - 1$  independent phases because of  $N_p - 1$  closed loops in the system. For simplicity, we only vary  $\phi_{I1}$  ( $= \phi$ ) and the other phases are set to zero. For single pathway ( $N_p = 1$ ), the efficiency  $P_{sink}$  is always equal to 0.695, this is due to the fact that no quantum interference can occur in single pathway. For double pathways ( $N_p = 2$ ), the quantum interference at site  $F$  occurs and the phases take effect. Due to the

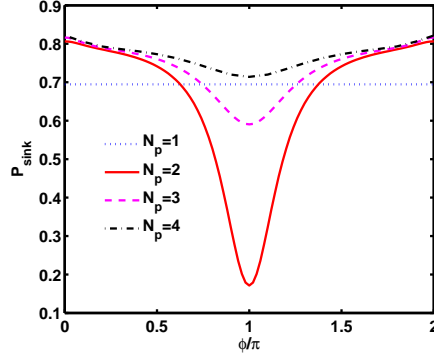


FIG. 5: (Color online) Transfer efficiency  $P_{sink}$  as a function of the phase difference  $\phi$  for different number  $N_p$  of the pathways. The other parameters are  $\Gamma = 1/100$ ,  $\gamma = 1/100$ ,  $\Gamma_s = 1/5$ , and  $V = 1/5$ .

destructive interference, there exists a minimal value of the transfer efficiency at  $\phi = \pi$ . The efficiency  $P_{sink}$  takes its maximal value at  $\phi = 0$  or  $2\pi$ , where the constructive interference occurs. The efficiency of multiple pathways at constructive interference has an enhancement compared with the single pathway. As the number of the pathways increases, the effects of destructive interference on the efficiency decrease. We here have assumed that all other phases in  $N_p > 3$  pathways are zero. If we further optimize those phases, the enhancement by the multiple-pathway are clearer. It supports the conclusion in quantum scattering model[28] where the resonance transport is enhanced in multiple-pathway. Therefore, the multiple-pathway can reduce the destructive interference and facilitate EET in quantum network. **It seems that most local minima or maxima occur at multiples of  $\pi/2$ , but the accumulated phases for local minima or maxima is the multiples of  $\pi/2$  only when all pathways are the same. The quantum interference at the given site is determined by the accumulated phase in the multiple pathways. When all pathways are the same, the constructive interference and the destructive interference occur at  $\phi = 0, \pi, 2\pi$ , respectively. However, when the pathways are not the same, the interference in the closed pathways becomes complicated. The phase conditions for the constructive interference and the destructive interference depend on the system parameters, such as the site energy, the coupling strength, and the number of the sites in each pathway.**

Note that the similar findings are also found in Ref.[30]. They defined an

effective hopping rate as the leading order picture and nonlocal kinetic couplings as the quantum correction and found that the optimized multiple pathways can suppress the destructive interference in nonlinear network configurations. Although the model and the method are different from ours, the impact of closed paths on the transport are the same in nature.

## V. EXCITATION ENERGY TRANSFER IN FMO COMPLEX

The architecture of antenna light-harvesting complexes varies widely among photosynthetic organisms. A well-studied example is the water-soluble FMO complex of green sulfur bacteria. The FMO complex essentially acts as a molecular wire, transferring excitation energy from the chlorosomes, which are the main light-harvesting antennae of green sulfur bacteria, to the membrane-embedded reaction center. The FMO is a trimer made of three identical subunits, each containing seven pigments[34]. Because the inter-subunit coupling is vanishingly small, we only consider the dynamics of the EET within one subunit. The subunit containing seven pigments shown in Fig. 6(a) can be modelled as a network of seven sites with site dependent coupling and site energies. We use the experimental Hamiltonian of FMO given in [33], and the matrix of the Hamiltonian takes the form

$$H = \begin{pmatrix} \mathbf{215} & -\mathbf{104.1} & 5.1 & -4.3 & 4.7 & -\mathbf{15.1} & -7.8 \\ -\mathbf{104.1} & \mathbf{220.0} & \mathbf{32.6} & 7.1 & 5.4 & 8.3 & 0.8 \\ 5.1 & \mathbf{32.6} & \mathbf{0.0} & -\mathbf{46.8} & 1.0 & -8.1 & 5.1 \\ -4.3 & 7.1 & -\mathbf{46.8} & \mathbf{125.0} & -\mathbf{70.7} & -14.7 & -\mathbf{61.5} \\ 4.7 & 5.4 & 1.0 & \mathbf{70.7} & \mathbf{450} & \mathbf{89.7} & -2.5 \\ -\mathbf{15.1} & 8.3 & -8.1 & -14.7 & \mathbf{89.7} & \mathbf{330.0} & \mathbf{32.7} \\ -7.8 & 0.8 & 5.1 & -\mathbf{61.5} & -2.5 & \mathbf{32.7} & \mathbf{280} \end{pmatrix} \quad (9)$$

with units of  $\text{cm}^{-1}$  and a total offset of  $12230\text{cm}^{-1}$  to set the lowest site energy to zero for convenience (This overall shift in energy does not affect the dynamics of the system). In units with  $\hbar = 1$ , we note that the rate  $1\text{ps}^{-1} \equiv 5.3 \text{ cm}^{-1}$ . By neglecting the couplings weaker than  $15 \text{ cm}^{-1}$  (only bold entries in the Hamiltonian are considered) in this model Hamiltonian, the transport in an individual monomer of FMO can be mapped to a quantum network shown in Fig. 6(b).

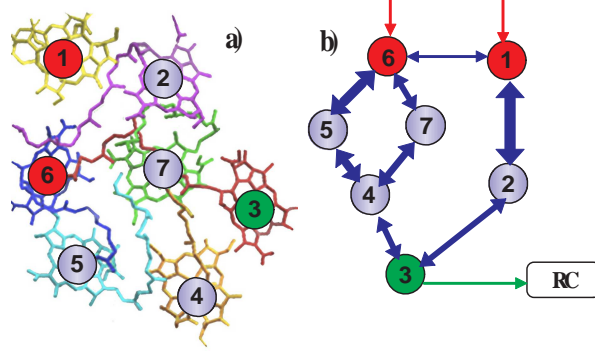


FIG. 6: (Color online)(a) The spatial structure of one monomeric subunit of the FMO complex [16, 21]. Each monomer has seven pigments labelled by ① – ⑦. The initial state is taken to be a superposition state located at the pigments 1 and 6. and pigment 3 is in the vicinity of the reaction center (RC). (b) The simplified network for the monomeric subunit of the FMO. The thickness of two-head arrow indicates the coupling strengths and only couplings above  $15 \text{ cm}^{-1}$  are shown. The exciton is transferred from sites 1 and 6 to site 3 through the network, and finally, trapped by the reaction center with the rate  $\Gamma_s$ .

However, the Hamiltonian in Eq.(9) may not be sufficient to describe the EET in the FMO. We here focus on the possible effects of the newly added phase factors in the coupling terms. From Eq. (2) and Fig. 6(b) we can find that there are eight phases,  $\phi_{12}, \phi_{23}, \phi_{34}, \phi_{45}, \phi_{47}, \phi_{56}, \phi_{67}, \phi_{16}$ , but only two phase differences,  $\phi_1 = \phi_{61} + \phi_{12} + \phi_{23} - \phi_{67} - \phi_{74} - \phi_{43}$  and  $\phi_2 = \phi_{67} + \phi_{74} - \phi_{65} - \phi_{54}$ , are independent since there are just two independent closed loops. Therefore, without loss of the generality, we vary the phases  $\phi_{12}$  and  $\phi_{67}$  and the other phases are set to zero in our numerical simulations.

The initial state for our simulation is a superposition state localized at pigments 1 and 6 which are close to the chlorosome antenna (donor). It can be written as  $|\Psi(0)\rangle = \alpha|1\rangle + \beta|6\rangle$  with  $|\alpha|^2 + |\beta|^2 = 1$ . The pigment 3 is the main excitation donor to the reaction center. The energy trapping rate from pigment 3 to the center in the literature [9–11] ranges from  $1 \text{ ps}^{-1}$  to  $4 \text{ ps}^{-1}$ . In our calculations, we chose  $\Gamma_s = 20/1.88 \text{ cm}^{-1}$  corresponding to about  $2 \text{ ps}^{-1}$ . The measured lifetime of excitons is of the order of  $1 \text{ ns}$  which determines a dissipative decay rate of  $0.5/188 \text{ cm}^{-1}$ . Unless otherwise noted, we choose  $\Gamma = 0.5/188 \text{ cm}^{-1}$  and  $\gamma = 0.01\Gamma$  in this paper and assume that  $\Gamma$  and  $\gamma$  are the same for each site. From Eqs. (2-7), we can numerically obtain the efficiency  $P_{sink}$  of the EET in FMO complex for different cases.

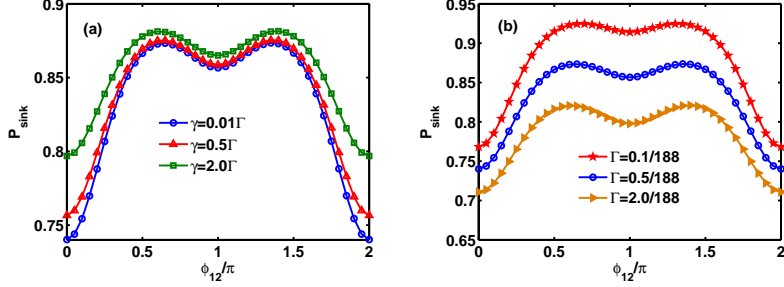


FIG. 7: (Color online) Transfer efficiency  $P_{sink}$  as a function of the phase  $\phi_{12}$ . (a) For different dephasing rates  $\gamma$  at  $\Gamma = 0.5/188 \text{ cm}^{-1}$ . (b) For different dissipative rates  $\Gamma$  at  $\gamma = 0.5/18800 \text{ cm}^{-1}$ . The other parameters are  $\Gamma_s = 20/1.88 \text{ cm}^{-1}$ ,  $\phi_{67} = 0$  and  $\alpha = \beta = \frac{\sqrt{2}}{2}$ .

Figure 7(a) and (b) shows the phase dependent efficiency for different dephasing and dissipative rates with  $\phi_{67} = 0$  and  $\alpha = \beta = \frac{\sqrt{2}}{2}$ . It is found that there exist two optimal values of  $\phi_{12}$  (e. g.  $\phi_{12} \approx \pi/2$  or  $3\pi/2$ ) at which the transfer efficiency  $P_{sink}$  takes its maximal value. When the dephasing rate  $\gamma$  or dissipative rate  $\Gamma$  varies, the shape of the curve in Fig. 7 almost does not change, which indicates an important feature that the optimized phases are not sensitive to the environment. The phases denote the distance between the pigments and the barriers between pigments, which are determined actually by the spatial distribution of seven pigments. When the pigments are optimally spaced, the exciton can pass through the FMO with optimal efficiency. Therefore, the phases from the two-body interactions play a key role in energy transfer of the FMO complex.

Figure 8 shows the dependence of the transfer efficiency  $P_{sink}$  on the phases  $\phi_{12}$  and  $\phi_{67}$  for different initial states. To study the significance of the phases, we can define the difference  $\Delta P$  between the maximal efficiency  $P_{sink}^{max}$  and the minimal efficiency  $P_{sink}^{min}$ ,  $\Delta P = P_{sink}^{max} - P_{sink}^{min}$ . We find that  $\Delta P = 0.2467$  for Fig. 8 (a) ( $\alpha = \beta = \frac{\sqrt{2}}{2}$ ),  $\Delta P = 0.6459$  for Fig. 8 (b) ( $\alpha = 0, \beta = 1$ ) and  $\Delta P = 0.1432$  for Fig. 8 (c) ( $\alpha = 1, \beta = 0$ ). Obviously, the phase can cause a significant change in the efficiency and the change just slightly depends on the initial states. The role of the phase coherence is to overcome local energetic traps and aid efficient trapping exciton energy by the pigments facing the reaction center. In this cases we can still find that there exist some optimal phase regions where the transfer efficiency takes its maxima. The optimal phase regions only slightly vary with the initial states. Therefore, we demonstrate that the phase plays a significant role in the EET and

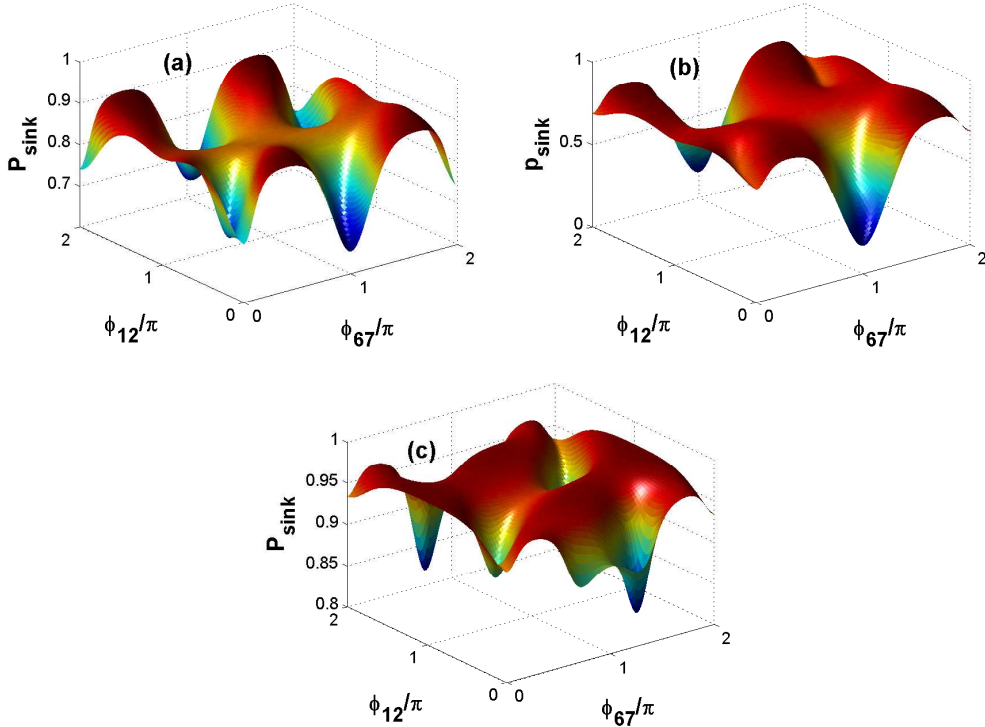


FIG. 8: (Color online) Transfer efficiency  $P_{sink}$  as a function of the phases  $\phi_{12}$  and  $\phi_{67}$  for different initial states. (a)  $\alpha = \beta = \frac{\sqrt{2}}{2}$ . (b)  $\alpha = 0$  and  $\beta = 1$ . (c)  $\alpha = 1$  and  $\beta = 0$ . The other parameters are  $\Gamma_s = 20/1.88 \text{ cm}^{-1}$ ,  $\gamma = 0.5/18800 \text{ cm}^{-1}$ , and  $\Gamma = 0.5/188 \text{ cm}^{-1}$ .

the optimal phase can facilitate the energy transfer in FMO complex.

The experimental evidences [2, 3] show that beside the optimal space distribution of the pigments, the multiple energy delivery pathway is another acceptable contributing factor for perfect energy transfer. Therefore, it is necessary to study the role of the multiple pathways in our model. In Fig. 9, the efficiency of one pathway is compared with that of the multiple pathways. It is found that the transfer efficiency  $P_{sink}$  gets a significant enhancement when the number of the pathways increases. The efficiency is only 0.6425 for single pathway, while it can reach 0.8 for multiple pathways. Remarkably, the efficiency in the full FMO (case III) even at destructive interference is larger than that in single pathway (case I). **This suggests that the dephasing noise in the system destroy the destructive interference and thus opens both paths for the transport [8, 10].** This result supports the conclusion in quantum scattering model[28] where the resonance transport is enhanced in multiple-pathway. Therefore, we can conclude that multiple pathways can also facilitate EET in

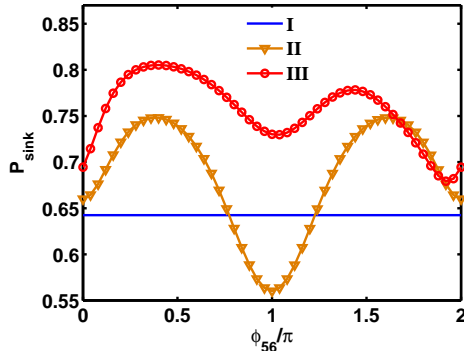


FIG. 9: (Color online) Transfer efficiency  $P_{sink}$  as a function of the phase  $\phi_{56}$  for different cases at  $\alpha = 0$  and  $\beta = 1$ . (I) One pathway:  $\textcircled{6} \rightarrow \textcircled{5} \rightarrow \textcircled{4} \rightarrow \textcircled{3}$ , namely,  $V_{12} = V_{23} = V_{16} = V_{67} = V_{47} = 0$ . (II) Two pathways:  $\textcircled{6} \rightarrow \textcircled{5} \rightarrow \textcircled{4} \rightarrow \textcircled{3}$  and  $\textcircled{6} \rightarrow \textcircled{7} \rightarrow \textcircled{4} \rightarrow \textcircled{3}$ , namely,  $V_{12} = V_{23} = V_{16} = 0$ . (III) Three pathways: the full quantum network of the FMO with  $\phi_{16} = 0.1\pi$ .  $\Gamma_s = 20/1.88 \text{ cm}^{-1}$ ,  $\gamma = 0.5/18800 \text{ cm}^{-1}$ , and  $\Gamma = 0.5/188 \text{ cm}^{-1}$ . The other phases are set to zero.

FMO complex which agrees with the experimental statement [2, 3].

## VI. CONCLUDING REMARKS

In this paper, we have investigated the efficiency of the EET in FMO complexes by adding the quantum phase factors to the quantum network model. The phase describes the length of the pigments, the distance and the barriers between pigments and is then determined by the space distribution of the pigments. We found that the optimal distribution of the pigments can lead to the high efficiency of the EET. Moreover, the optimal phase is not sensitive to the environments. If the distribution of the pigments is optimized, the efficiency always takes its maximal value, which is indeed significant for high transfer efficiency. As we know, the biological system governed by Darwinian selection has the optimal structure, which can ensure that the quantum coherence occurs in the optimal spatial distribution. In addition, we also find that the multiple-pathway can facilitate EET in FMO complex. Therefore, we can conclude from the studies of the complex quantum network model that, the optimal space distribution of the pigments, the multitude of energy delivery pathways and the quantum effects, are combined together to contribute to the perfect energy transport in the FMO complexes.

In this paper we just add the phase factors phenomenally to the two-body couplings in the Hamiltonian (9). Qualitatively, the quantum phases are determined by the spatial structure of the pigments in photosynthetic complexes; however, how to determine them quantitatively in a microscopic theory or from the experimental measurements is an important open question which deserves further study.

Though we only have studied the transport process through the FMO protein, the methods and conclusions can be extended to other photosynthetic light-harvesting complexes. Furthermore, understanding the mechanism of efficient energy transfer in natural light-harvesting systems can help developing low-cost and highly-efficient man-made solar energy apparatus, including photovoltaic devices and artificial photosynthesis.

This work was supported by the NNSFC (Nos.11175067, and 11125417), the SKPBRC (No.2011CB922104), and the NSF of Guangdong (No.S2011010003323).

*Note added.* – Shortly after we submitted the paper, there was a preprint pasted in arXiv[36], where the effects of the complex coupling are discussed.

### Appendix A: The derivation of Eq. (8)

In terms of the density matrix elements in the site basis  $\rho_{ij}(t)$ , the equations of motion for  $N = 3$  are

$$\frac{d\rho_{ij}}{dt} = -[2\Gamma + \Gamma_s(\delta_{iN} + \delta_{jN} + 2\gamma - 2\gamma\delta_{ij})]\rho_{ij} + iV[\sum_{l \neq j} e^{-i\phi_{il}} \rho_{il} - \sum_{l \neq i} e^{i\phi_{lj}} \rho_{lj}], \quad (\text{A1})$$

$$\frac{d\rho_{sink}}{dt} = 2\Gamma_s \rho_{33}. \quad (\text{A2})$$

Since the exciton is transferred from site 1 to site 3, the initial conditions are

$$\rho_{11}(0) = 1, \rho_{sink}(0) = 0, \quad (\text{A3})$$

and the other density matrix elements  $\rho_{ij} = 0$ .

The system of coupled differential equations can be converted into a set of algebraic equations via the Laplace transform. The above equations can be rewritten by the following set of equations for the Laplace s-domain variables, for  $\tilde{\rho}_{11}$

$$(s + 2\Gamma)\tilde{\rho}_{11} - 1 - iV\left[\sum_{l \neq j} e^{-i\phi_{il}} \tilde{\rho}_{il} - \sum_{l \neq i} e^{i\phi_{lj}} \tilde{\rho}_{lj}\right] = 0, \quad (\text{A4})$$

and the other density matrix elements are

$$[s + 2\Gamma + \Gamma_s(\delta_{iN} + \delta_{jN} + 2\gamma - 2\gamma\delta_{ij})\tilde{\rho}_{ij} - iV\left[\sum_{l \neq j} e^{-i\phi_{il}} \tilde{\rho}_{il} - \sum_{l \neq i} e^{i\phi_{lj}} \tilde{\rho}_{lj}\right]] = 0, \quad (\text{A5})$$

$$s\tilde{\rho}_{sink}(s) - 2\Gamma_s\tilde{\rho}_{33} = 0. \quad (\text{A6})$$

From Eqs. (A4-A6), we can easily obtain the expression of  $\tilde{\rho}_{sink}(s)$ . From the relation of the Laplace transform for  $t$  and  $s$ , we can find that

$$P_{sink} = \rho_{sink}(\infty) = \lim_{s \rightarrow 0} s\tilde{\rho}_{sink}(s), \quad (\text{A7})$$

and then the Eq. (8) is obtained.

- 
- [1] G. D. Scholes, G. R. Fleming, A. Olaya-Castro and R. V. Grondelle, *Nature Chemistry* **3**, 763 (2011); Y. C. Cheng and G. R. Fleming, *Annu. Rev. Phys. Chem.* **60**, 241 (2009).
  - [2] R. V. Grondelle and V. I. Novoderezhkin, *Nature (London)* **463**, 614 (2010); R. V. Grondelle, J. P. Dekker, T. Gillbro, and V. Sundstrom, *Biochim. Biophys. Acta* **1187**, 1 (1994).
  - [3] M. K. Sener, J. D. Olsen, C. N. Hunter, and K. Schulten, *Proc. Natl. Acad. Sci. USA* **104**, 15723 (2007).
  - [4] G. S. Engel, T. R. Calhoun, E. L. Read, T. K. Ahn, T. Manal, Y. C. Cheng, R. E. Blankenship, and G. R. Fleming, *Nature (London)* **446**, 782 (2007).
  - [5] H. Lee, Y. C. Cheng, and G. R. Fleming, *Science* **316**, 1462 (2007).
  - [6] E. Collini, C. Y. Wong, K. E. Wilk, P. M. G. Curmi, P. Brumer, and G. D. Scholes, *Nature (London)* **463**, 644 (2010).
  - [7] G. Panitchayangkoona, D. Hayesa, K. A. Fransteda, J. R. Carama, E. Harela, J. Wenb, R. E. Blankenshipb, and G. S. Engel, *Proc. Natl. Acad. Sci. USA* **107**, 12766 (2010).
  - [8] M. B. Plenio and S. F. Huelga, *New J. Phys.* **10**, 113019 (2008); M. Mohseni, P. Rebentrost, S. Lloyd and A. Aspuru-Guzik, *J. Chem. Phys.* **129**, 174106 (2008).
  - [9] S. Hoyer, M. Sarovar, and K. B. Whaley, *New J. Phys.* **12**, 065041(2010); F. Fassioli and A. Olaya-Castro, *New J. Phys.* **12**, 085006(2010).

- [10] F. Caruso, A. W. Chin, A. Datta, S. F. Huelga and M. B. Plenio, *J. Chem. Phys.* **131**, 105106 (2009); F. Caruso, S. Montangero, T. Calarco, S. F. Huelga, M. B. Plenio, *Phys. Rev. A* **85**, 042331 (2012).
- [11] A. W. Chin, A. Datta, F. Caruso, S. F. Huelga and M. B. Plenio, *New J. Phys.* **12**, 065002 (2010).
- [12] G. Panitchayangkoon, D. Hayes, K. A. Fransted, J. R. Caram, E. Harel, J. Wen, R. E. Blankenship and G. S. Engel, *Proc. Natl. Acad. Sci. USA* **107**, 12766 (2010).
- [13] Y. C. Cheng and R. J. Silbey, *Phys. Rev. Lett.* **96**, 028103 (2006).
- [14] A. Nazir *Phys. Rev. Lett.* **103**, 146404 (2009).
- [15] T. R. Calhoun, N. S. Ginsberg, G. S. Schlau-Cohen, Y. C. Cheng, M. Ballottari, R. Bassi and G. R. Fleming, *J. Phys. Chem. B* **113**, 16291(2009).
- [16] P. Rebentrost, M. Mohseni, I. Kassal, S. Lloyd and A. Aspuru-Guzik, *New J. Phys.* **11**, 033003 (2009); P. Rebentrost, M. Mohseni and A. Aspuru-Guzik, *J. Phys. Chem. B* **113**, 9942(2009).
- [17] L. James, R. Junghee, L. Changhyoup, Y. Seokwon, J. Hyunseok and L. Jinhyoung, *New J. Phys.* **13**, 103002 (2011).
- [18] B. Cui, X. X. Yi, C. H. Oh, *J. Phys. B: At. Mol. Opt. Phys.* **45**, 085501 (2012); B. Cui, X. Y. Zhang, X. X. Yi, arXiv:1106.4429.
- [19] A. K. Ringsmuth, G. J. Milburn, and T. M. Stace, *Nature Physics* **8**, 562 (2012).
- [20] T. Scholak, F. Melo, T. Wellens, F. Mintert, and A. Buchleitner, *Phys. Rev. E* **83**, 021912 (2011).
- [21] M. Sarovar, A. Ishizaki, G. R. Fleming, and K. Birgitta Whaley, *Nature Physics* **6**, 462 (2010); A. Ishizaki and G. R. Fleming, *Proc. Natl. Acad. Sci. USA* **106**, 17255(2009).
- [22] A. Ishizaki and G. R. Fleming, *J. Chem. Phys.* **130**, 234111 (2009).
- [23] S. Yang, D. Z. Xu, Z. Song, and C. P. Sun, *J. Chem. Phys.* **132**, 234501 (2011); J. Q. Liao, J. F. Huang, L. M. Kuang, C. P. Sun, *Phys. Rev. A* **82**, 052109 (2010); H. Dong, D. Z. Xu, C. P. Sun, *Light: Science and Applications* (2012) 1.
- [24] K. G. Pulak, Y. S. Anatoly, and N. Franco, *J. Chem. Phys.* **134**, 244103 (2011)
- [25] J. S. Cao, *J. Chem. Phys.* **107**, 3204 (1997); J. L. Wu, F. Liu, Y. Shen, J. S. Cao, R. J. Silbey, *New J. Phys.* **12**, 105012 (2010); J. Ye, K. Sun, Y. Zhao, Y. Yu, C. K. Lee, J. S. Cao, *J. Chem. Phys.* **136**, 245104 (2012).
- [26] J. Prior, A.W. Chin, S. F. Huelga, M. B. Plenio, *Phys. Rev. Lett.* **105**, 050404 (2010).

- [27] X. T. Liang, Phys. Rev. E **82**, 051918 (2010) ; X. T. Liang, W. M. Zhang, and Y. Z. Zhuo, Phys. Rev. E **81**, 011906 (2010).
- [28] B. Q. Ai and S. L. Zhu, arXiv:1201.1740.
- [29] Y. Y. Jing, R. H. Zheng, H. X. Li, and Q. Shi, J. Phys. Chem. B **116**, 1164 (2012); P. K. Ghosh, A. Y. Smirnov, and F. Nori, J. Chem. Phys. **134**, 244103 (2011); P. K. Ghosh, A. Y. Smirnov, and F. Nori, J. Chem. Phys. **131**, 035102 (2009); G. Ritschel, J. Roden, W. T. Strunz, and A. Eisfeld, New J. Phys. **13**, 113034 (2011).
- [30] J. S. Cao and R. J. Silbey, J. Phys. Chem. A **113**, 13825 (2009); A. Kelly and Y. M. Rhee, J. Phys. Chem. Lett. **2**, 808 (2011).
- [31] N. Christensson, H. F. Kauffmann, T. Pullerits, T. Mancal, arXiv:1201.6325; A. W. Chin, J. Prior, R. Rosenbach, F. Caycedo-Soler, S. F. Huelga, M. B. Plenio, arXiv:1203.0776.
- [32] For a review, see S. Gnutzman and U. Smilansky, Adv. Phys. **55**, 527 (2006).
- [33] J. Adolphs and T. Renger, Biophys. J. **91**, 2778 (2006).
- [34] An additional (the eighth) pigment was recently discovered in each subunit. However, we ignore this pigment since the eighth pigment is only loosely bound and it usually detaches from the others when the system is isolated from its environment to perform experiments, see Ref.[35]. In addition, the main conclusions obtained here are essentially the same for both eight and seven pigments.
- [35] A. Ben-Shem, F. Frolow, N. Nelson, FEBS Lett. **564**, 274 (2004); J. Wen, H. Zhang, M. L. Gross, and R. E. Blankenship, Biochemistry **50**, 3502 (2011); D. E. Tronrud, J. Wen, L. Gay, R. E. Blankenship, Photosynth. Res. **100** 79 (2009); M. Schmidt am Busch, F. Muh, M. El-Amine Madjet, and T. Renger, J. Phys. Chem. Lett. **2**,93 (2011).
- [36] X. X. Yi, X. Y. Zhang, and C. H. Oh, arXiv:1208.4671 (unpublished).